Nephron

Clinical Practice

Nephron
DOI: 10.1159/000544709

Received: June 16, 2024
Accepted: February 6, 2025
Published online: February 13, 2025

Membranoproliferative Glomerulonephritis with Striated Ultrastructural Deposits with Significantly Elevated Fibrinogen and Fibronectin on Mass Spectrometry Analysis: A Case Report and Literature Review

Manna Ishida[a] Shinya Yamamoto[a] Yohei Iwashige[a] Shuma Miyazawa[a] Hirosuke Nakata[a] Koichi Seta[d] Kensei Yahata[d] Sachiko Minamiguchi[b] Yoko Endo[e] Akiko Mii[e] Akira Shimizu[f] Motoko Yanagita[a, c]

[a]Department of Nephrology, Kyoto University, Kyoto, Japan; [b]Department of Diagnostic Pathology, Kyoto University, Kyoto, Japan; [c]Institute for the Advanced Study of Human Biology (WPI-ASHBi), Kyoto University, Kyoto, Japan; [d]Department of Nephrology, National Hospital Organization Kyoto Medical Center, Kyoto, Japan; [e]Department of Nephrology, Nippon Medical School, Tokyo, Japan; [f]Department of Analytical Human Pathology, Nippon Medical School, Tokyo, Japan

Keywords
Membranoproliferative glomerulonephritis · Fibrinogen · Fibrin · Fibronectin · Deposit · Mass spectrometry

Abstract
Glomerular diseases with organized deposits can be classified into various etiologies. A diagnostic algorithm based on clinical and pathological findings has been proposed. However, some cases cannot be diagnosed using existing algorithms. Here, we report the case of a 77-year-old man diagnosed with membranoproliferative glomerulonephritis (MPGN) with striated ultrastructural deposits, microfilament-like substructures with straight bands arranged in parallel in the subendothelial space by two sequential renal biopsies. His examinations and clinical findings were incompatible with known glomerular diseases with organized deposits. Dialysis was initiated 10 months after the second biopsy procedure. Furthermore, we report the first mass spectrometry analysis of laser micro-dissected glomeruli with striated ultrastructural deposits, which revealed significant levels of fibrinogen and fibronectin. Immunostaining was positive for fibrinogen, fibrin, and fibronectin in the subendothelial space. These findings suggest that the deposits were composed of a fibrin-fibronectin complex and that accumulation of these fibrin-fibronectin complexes possibly induced endothelial injury, leading to MPGN. We also reviewed the literature on the clinical and pathological characteristics of the four cases with striated ultrastructural deposits. Our investigation showed that all patients had the MPGN pattern and striated ultrastructural deposits in the subendothelial space, and all underwent hemodialysis

Manna Ishida and Shinya Yamamoto contributed equally to this work.
The present address of Kensei Yahata is Department of Nephrology, Osaka Red Cross Hospital, Osaka, Japan.
The present address of Yoko Endo is Department of Pathology, Tokyo Yamate Medical Center, Tokyo, Japan.

karger@karger.com
www.karger.com/nef

Correspondence to:
Shinya Yamamoto, syamamon@kuhp.kyoto-u.ac.jp

within 3 years of renal biopsy. Clinicians should be aware of the findings of glomerulonephritis with striated ultrastructural deposits since this disease may be a new entity and has a poor prognosis.

Introduction

Glomerular diseases with organized deposits are classified into amyloidosis and non-amyloid glomerulopathy, including various etiologies such as fibrillary glomerulonephritis, immunotactoid glomerulopathy, cryoglobulinemic glomerulonephritis, collagenofibrotic glomerulopathy, and fibronectin nephropathy. The evaluation of renal diseases with organized deposits requires clinical history, laboratory data, and detailed histological analysis. Information on specific staining, patterns of immunoglobulin staining, and electron microscopic findings are crucial in distinguishing between these diseases [1]. A diagnostic algorithm based on clinical and pathological findings has been proposed [2]. However, we sometimes encounter cases that cannot be diagnosed using the existing algorithms. These cases could represent an unclassified group of diseases. The present case is characterized by non-amyloid and non-immunoglobulin-derived glomerulonephritis with no family history of kidney disease. Non-amyloid and non-immunoglobulin-derived glomerulonephritis with organized deposit include diabetic sclerosis, collagenofibrotic glomerulopathy, and fibronectin nephropathy, but these diseases are not consistent with this case on clinical and pathological findings.

Recently, proteomics has been introduced to analyze the pathophysiology of kidney biopsy specimens [3], especially for amyloid, allowing us to determine the composition of deposits and select appropriate treatments [4, 5]. Therefore, it could be useful to apply mass spectrometry (MS) to undiagnosed glomerular diseases with organized deposits.

Here, we describe the long-term clinical course of a case of progressive membranoproliferative glomerulonephritis (MPGN) with striated ultrastructural deposits, which had regularly stacked straight electron-dense bands arranged in parallel, confirmed by two sequential biopsies. Furthermore, we report the first MS analysis of laser micro-dissected glomeruli with striated ultrastructural deposits. In addition, we present a literature review on clinical and pathological features of four cases characterized by striated ultrastructural deposits.

Case Report

A 77-year-old Japanese man presented to our hospital with proteinuria, hematuria, and lower-leg edema. The initial onset of symptoms occurred 1 month earlier. His body weight had increased by 4.9 kg within the past month. The patient had no relevant family history, and he had a medical history of prostate cancer surgery. His regular medication included edoxaban for atrial fibrillation. On admission, his blood pressure was 126/65 mm Hg, temperature was 36.5°C, and pulse rate was 70 beats/min. Physical examination revealed lower extremity edema. Laboratory tests showed that serum creatinine was 0.85 mg/dL, C-reactive protein (CRP) was 0.4 mg/dL, serum total protein was 5.8 g/dL, and serum albumin was 3.3 g/dL. Prothrombin time-international normalized ratio (PT-INR) was 1.57, and other coagulation systems, including activated partial thromboplastin time (APTT), thrombin, and plasmin were normal. M-protein was not detected. Tests for hepatitis virus B, C, and HIV were negative. Maintaining the appropriate temperature is crucial for optimizing the yield of cryoglobulins in subsequent analysis. We maintained the sample at 37°C during storage and transport, but could not detect cryoglobulin. Cryofibrinogen and Bence-Jones protein were also negative. Urinalysis revealed high proteinuria (2.3 g/g Cr) and dysmorphic hematuria (Table 1). Bone marrow biopsy showed mild myelodysplasia that did not require treatment.

The specimen of the renal biopsy contained 28 glomeruli, two of which were globally sclerosed. Mesangial matrix expansion, segmental lobular configuration with mesangial and endocapillary hypercellularity, and partial double-contour formation were apparent (Fig. 1a–c). No obvious tubulointerstitial inflammation or vascular damage was observed. Congo red staining was negative. Light microscopic findings were consistent with MPGN. Immunofluorescence (IF) staining of frozen sections showed that IgM, C3, and fibrinogen were positive in mesangium and partially along capillary wall whereas IgG was negative (Fig. 1d–f). The kappa light chain staining was slightly positive nonspecifically, and the positive area was very partial. Lambda light chain staining was negative. IF on paraffin-embedded sections of IgG with proteinase K digestion was also negative. Although immunostaining for C3 was partially positive, genetic abnormalities in the complement genes were not detected. The immunostaining of collagen type VI was not positive in the subendothelial space, which indicated that collagen VI was not involved in the ultrastructural deposits (online suppl. Fig. 1a, b; for all online suppl. material, see https://doi.org/10.1159/000544709). Electron microscopy (EM) revealed

Table 1. Laboratory data

Laboratory tests			
Complete blood count		*Immunology*	
White blood cell, 10^3/μL	3.04	Immunoglobulin G, mg/dL	1,141
Red blood cells, 10^6/μL	3.48	Immunoglobulin A, mg/dL	150
Hemoglobin, g/μL	11.7	Immunoglobulin M, mg/dL	110
Hematocrit, %	36.2	Complement 3, mg/dL	75
Platelets, 10^3/μL	116	Complement 4, mg/dL	22.1
Coagulation system		CH50, CH50/mL	38
PT, %	83	Antinuclear antibody	40
PT-INR	1.57	Rheumatoid factor, IU/mL	8.0>
APTT, s	30.6	Cryoglobulin	–
Fibrinogen, mg/dL	271	Cryofibrinogen	–
D-dimer, μg/mL	0.4	Anti-GBM antibody	<2.0
AT-III	92.4	MPO-ANCA	<1
TAT, ng/dL	1.2	PR3-ANCA	<1
PIC, μg/mL	1.1	Free light chain κ, mg/L	67.6
Chemistry		Free light chain λ, mg/L	32.9
Aspartate aminotransferase, IU/L	31	FLC κ/λ	2.06
Alanine aminotransferase, IU/L	18	Bence-Jones protein	Negative
Alkaline phosphatase, IU/L	74	*Infection*	
Gamma glutamyl transpeptidase, IU/L	34	HBsAg	–
Lactate dehydrogenase, IU/L	242	HBsAb	–
Total cholesterol, mg/dL	163	HbcAb	–
Choline esterase, IU/L	209	HCVAb	–
Total bilirubin, mg/dL	1	TP Ab	–
Total protein, g/dL	5.8	HIV	–
Albumin, g/dL	3.3	T-SPOT	–
Blood urea nitrogen, mg/dL	20	QuantiFERON-TB	Negative
Creatinine, mg/dL	0.85	*Urinalysis*	
eGFR, mL/min/1.73 m^2	66.6	Specific gravity	1.016
Creatine kinase, IU/L	95	pH	5.5
Uric acid, mg/dL	6.9	Protein	2+
Sodium, mEq/L	143	Occult blood	3+
Potassium, mEq/L	4.5	B2-microglobulin, μg/mL	0.053
Chloride, mEq/L	106	NAG, IU/L	14.7
Calcium, mEq/L	8.6	24 h proteinuria, g/24 h	1.2
Phosphate, mEq/L	2.8	*Urine sediment*	
Glucose, mg/dL	79	Erythrocytes/HPF, dysmorphic	20–29
C-reactive protein, mg/dL	0.1	Leukocytes/HPF	5–9
HbA1c, %	5.6		
BNP, pg/mL	89.7		

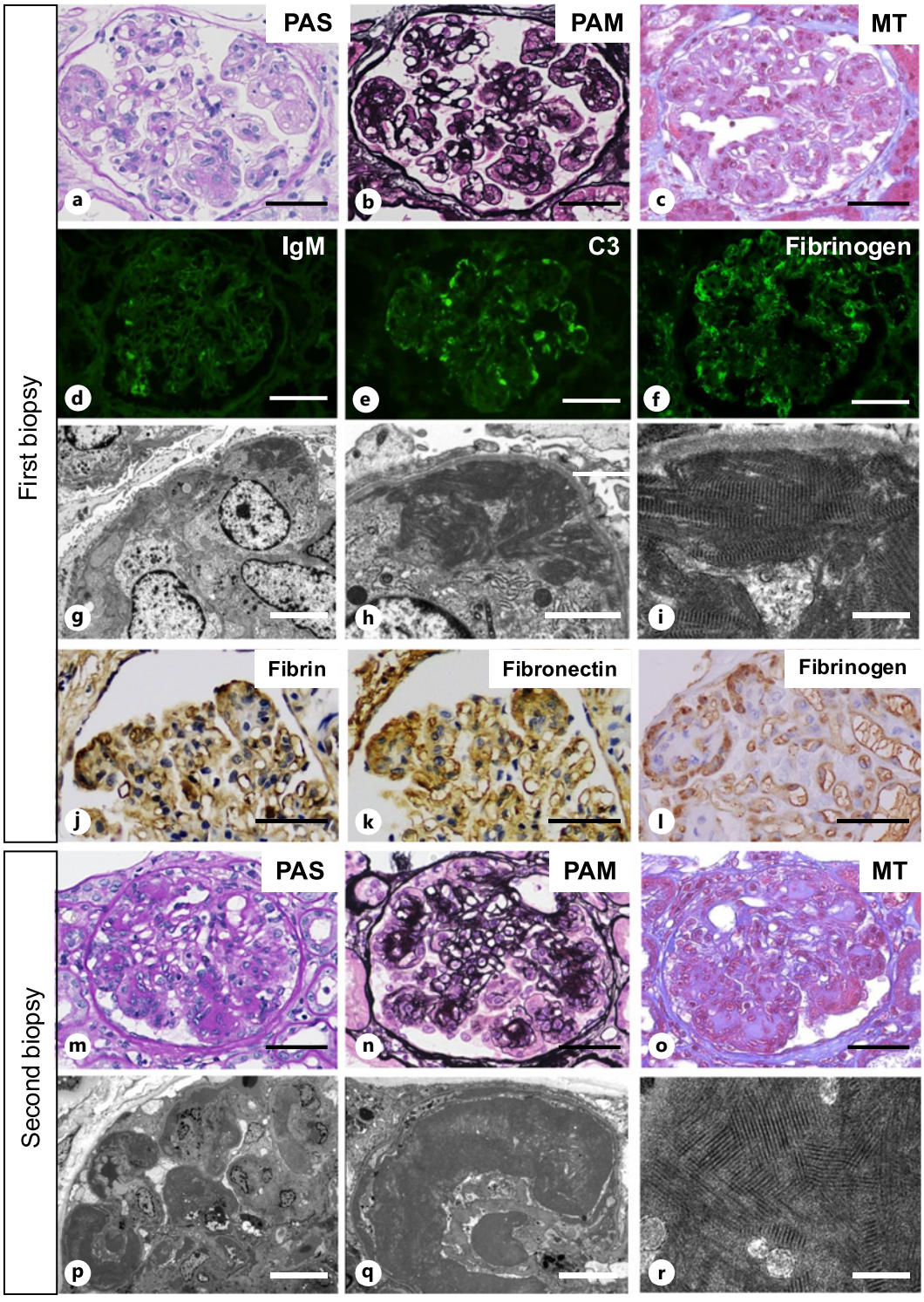

1

(For legend see next page.)

foot process effacement and organized deposits with striated ultrastructure in the subendothelial space (Fig. 1g–i). The distribution of these deposits was segmental. Most deposits contained micro-filament-like substructures with regularly stacked, straight electron-dense bands arranged in parallel. The electron-dense bands were 10–12 nm wide, with a distinctive periodicity of approximately 20–30 nm. Based on the serological and pathological findings, we excluded cryoglobulinemic glomerulonephritis, cryofibrinogen-associated glomerulonephritis, immunotactoid glomerulonephritis, fibrillary glomerulonephritis, lupus nephritis, and type VI collagen-related nephropathy.

We also performed laser microdissection of the glomeruli followed by liquid chromatography-tandem MS to determine the composition of the striated ultrastructural deposits, and we also estimated the absolute protein amount by exponentially modified protein abundance (emPAI) [6]. The MS analysis and emPAI showed that fibrinogen and fibronectin levels were significantly increased (Fig. 2a). To confirm the localization of these components in the glomeruli, immunostaining for fibrinogen, fibrin, and fibronectin was performed on the paraffin sections; all were positive in the subendothelial space (Fig. 1j–l). These results indicate that fibrinogen, fibrin, and fibronectin could be involved in the formation of the deposit structure.

After we initiated diuretics without immunosuppressive drugs, the patient's fluid retention improved, and he was discharged. However, he was readmitted with dyspnea due to volume overload 23 months after the first biopsy. His creatinine level had increased to 1.78 mg/dL, and proteinuria had increased to 11.3 g/g Cr. Cryoglobulin, cryofibrinogen, and Bence-Jones protein were all negative. Laboratory re-examination and a second bone marrow biopsy revealed no evidence of malignancy or hematologic disorders. A second renal biopsy revealed severe mesangial matrix expansion, global lobular configuration with mesangial and endocapillary hypercellularity, and remarkable enlargement of the subendothelial space in all the glomeruli (Fig. 1m–o). IF staining of frozen sections showed that the kappa and lambda light chain results were negative, and IgM positive area was very partial. The intensity of IgM staining was weaker in 2nd biopsy sample than in 1st biopsy sample. Given that the glomerulonephritis in the present case exhibited progressive deterioration over time, it is plausible to presume that IgM deposition does not play a significant role in the pathogenesis. In addition, intraluminal thrombi or cryoglobulinemic vasculitis were not observed. These findings were not consistent with a diagnosis of cryoglobulinemic glomerulonephritis. EM revealed marked expansion of the area occupied by the striated ultrastructural deposits, indicating that the glomerulonephritis had progressed over 2 years (Fig. 1p–r). Immunostaining for fibrinogen, fibrin, and fibronectin were all positive in the subendothelial space (online suppl. Fig. 2a–c). He was started on high-dose steroids but did not respond. Dialysis was initiated 10 months after the second biopsy procedure.

Materials and Methods

Mass Spectrometry

5-μm-thick sections of 20% formalin-fixed paraffin-embedded tissues were dissected by LMD using the Leica dissector (Leica LMD6000; Leica Microsystems, Mannheim, Germany) [7]. Micro-dissected tissue samples were collected in 0.5 mL microcentrifuge tube caps containing 40 μL Tris/EDTA/0.002% Zwittergent 3–16 buffer. After heating at 98°C for 90 min, the samples were sonicated at 35 kHz using a sonicator (Transsonication 890, Elma Schmidbauer GmbH, Singen, Germany) in a water bath for 90 min. The micro-dissected tissues were digested overnight with tryptic peptides at 37°C. After digestion, the samples with dithiothreitol were heated to 95°C for 5 min. After tissue digestion, all samples were analyzed by LCMS/MS using an amaZon ETD (Bruker Daltonics, Billerica, MA, USA). Raw data files from the

Fig. 1. Renal histological findings. **a–c** Partial mesangial and endocapillary hypercellularity and double-contour formation were shown in the first biopsy (periodic acid-Schiff stain (**a**), periodic acid-methenamine-silver stain (**b**), Masson's trichrome stain (**c**)). **d–f** Immunofluorescence revealed focal granular staining of IgM, C3, and fibrinogen in the mesangium and along the capillary wall. **g–i** Electron microscopy showed foot process effacement and organized deposits with striated ultrastructural deposits in the subendothelial space. The electron-dense bands were 10–12 nm wide and 20–30 nm from center to center. **j–l** Immunohistochemical staining for fibrin, fibronectin, and fibrinogen were all positive in subendothelial space. **m–o** The second biopsy revealed global mesangial and endocapillary hypercellularity and double-contour formation in almost all glomeruli (periodic acid-Schiff stain (**m**), periodic acid-methenamine-silver stain (**n**), Masson's trichrome stain (**o**)). **p–r** EM from the second biopsy revealed marked expansion of the area occupied by the striated ultrastructural deposits. **a–f**, **j–o** Bars = 50 μm. **g**, **p** Bars = 10 μm. **h** Bar = 2 μm. **q** Bar = 5 μm. **i**, **r** Bars = 500 nm.

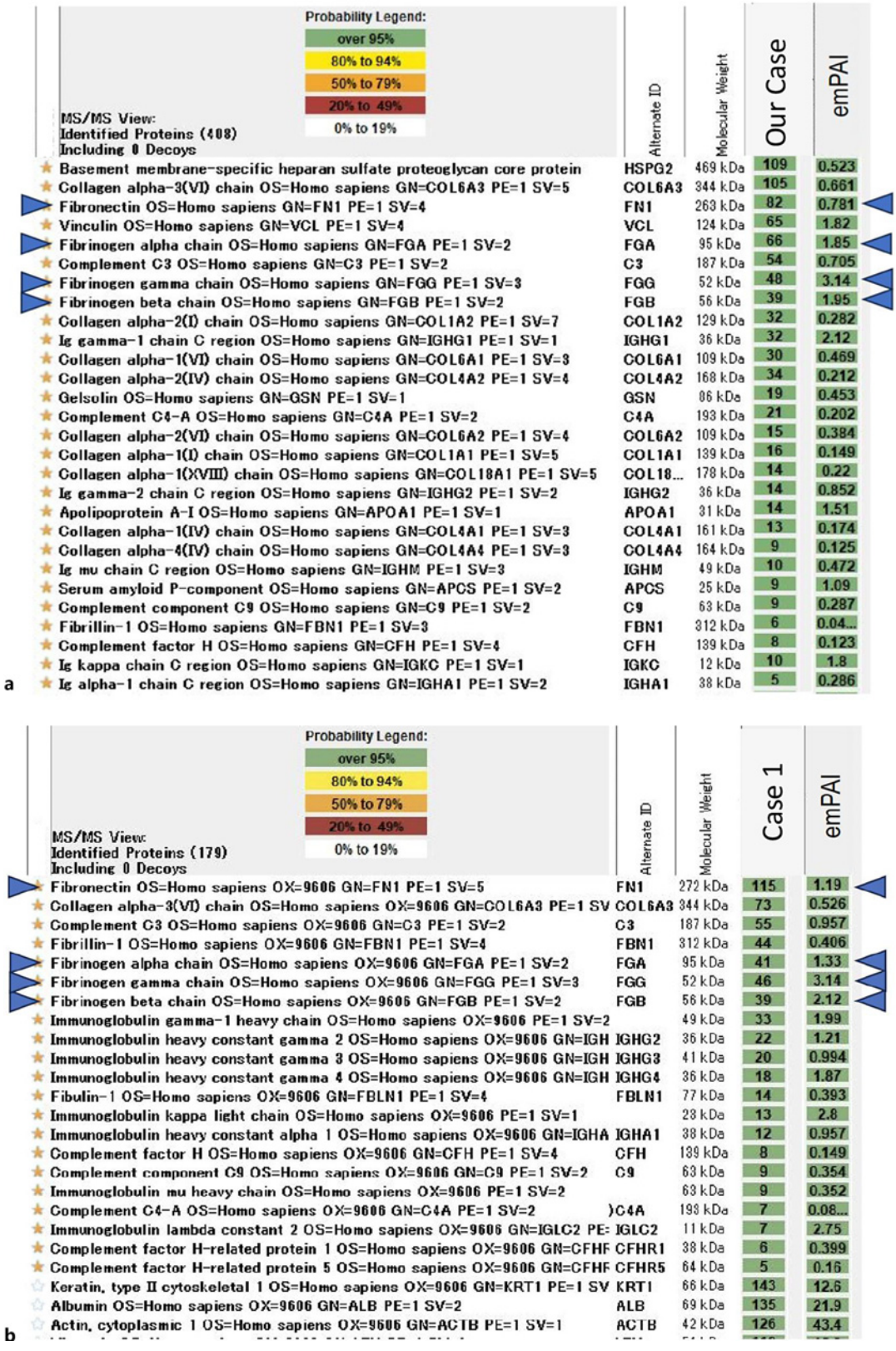

2

(For legend see next page.)

LCMS/MS were queried using two different algorithm databases (Mascot and X!Tandem). The results were combined, and the peptide and protein probability scores were assigned according to the Scaffold database derived from the SwissProt human database (Proteome Software Inc., Portland, OR, USA). The spectra value indicates the total number of mass spectra collected by LCMS/MS and matches the protein determined when using the proteomics software. A higher mass spectra number is indicative of greater abundance and higher confidence in protein identification [7].

Immunohistochemistry

Paraffin-embedded tissue sections were rehydrated, and endogenous peroxidase was blocked using 3% hydrogen peroxide in methanol. The following primary antibodies were used for immunostaining: anti-fibrinogen (catalog no. A 0080; DAKO), anti-fibronectin (catalog No. A 0245; DAKO), anti–Fibrin (catalog no. MABS 2155; Merck), and collagen type VI polyclonal antibody (17023-1-AP: Proteintech, USA).

Discussion

Here, we report a rare case of MPGN with striated ultrastructural deposits. Notably, the present case is inconsistent with known diseases characterized by the organized deposition of microfibrillar or microtubular structures. MS and immunostaining analyses suggested that fibrinogen, fibrin, and fibronectin were involved in ultrastructure formation. In addition, findings from two sequential biopsies indicated that the ultrastructural deposition is an important factor in disease progression.

Pathological findings showing micro-filament-like substructures were highly characteristic of this case. We excluded known glomerular diseases with organized deposits (Fig. 3). First, our case is classified into non-amyloid glomerulonephritis. Next, this case is categorized into non-immunoglobulin-derived glomerulonephritis because we did not detect significant immunoglobulin or complement deposition by IF staining. Our patient had no diabetes or family history of kidney disease. The appearance and size of the electron-dense bands were not

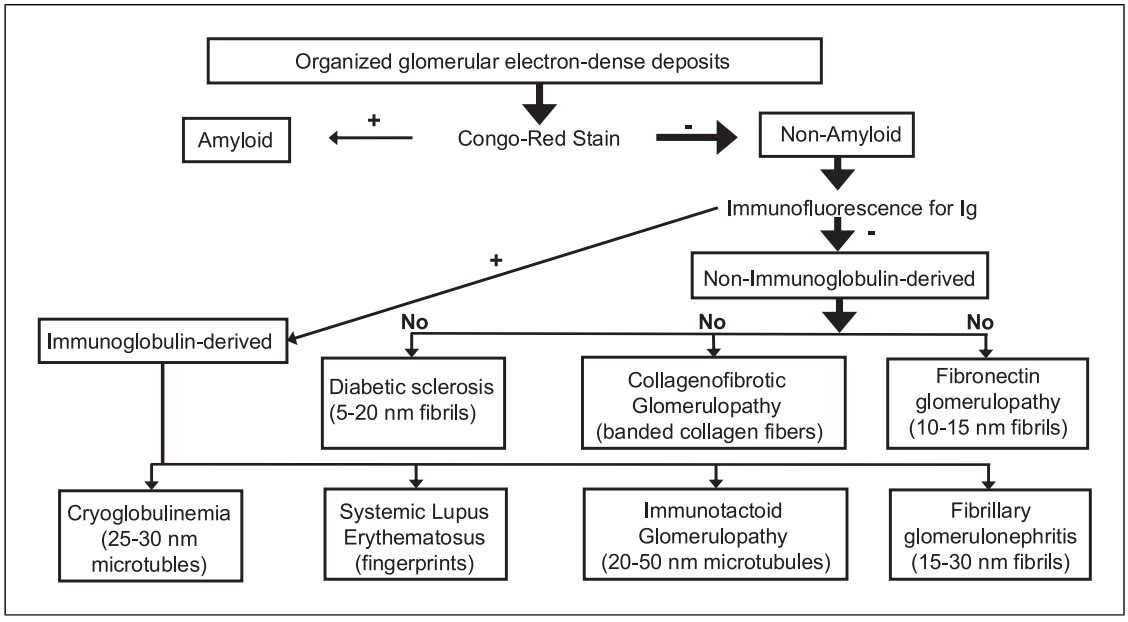

Fig. 3. A diagnostic algorithm for glomerular diseases with organized deposits.

Fig. 2. Mass spectrometry (MS) data. We present MS data in our case (**a**) and an additional case (case 1) (**b**). The MS result of the additional case was provided by National Hospital Organization Kyoto Medical Center. Each number of the right-most column corresponds to the number of tandem MS spectra associated with the protein in the samples, which is a surrogate measure of abundance. Proteins with five or more spectra were used for clinical interpretation. Fibrinogen and fibronectin were detected at high levels in both cases. Furthermore, we estimated the absolute protein amount by emPAI, which confirmed that fibrinogen and fibronectin are significantly detected.

Nephron
DOI: 10.1159/000544709

Table 2. Clinical and pathological characteristics of four cases from the literature with striated ultrastructural deposits

Case	Race	Sex	Age	Family history	Clinical presentation	Medical history	Proteinuria	Hematuria	Cr, mg/dL	M-protein	Treatment	Clinical course
(a)												
1 [10]	Japanese	M	71	ND	Hypertension Edema	Arteriosclerosis, smoking	13 g/gCr	55–99 (/HPF)	1.0	(–)	Conservative treatment	HD (9 months after biopsy)
2 [11]	Japanese	F	62	No	Proteinuria Edema	Hypertension, smoking	6.2 g/day	ND	0.6	(–)	Pulse steroid therapy, PSL40 mg/day	HD (23 months after biopsy)
3 [12]	Japanese	M	68	No	Proteinuria Edema	Hypertension	1.4 g/day	10–19 (/HPF)	1.3	(–)	PSL20 mg/day	HD (3 years after biopsy)
4-1st [13]	Japanese	M	64	No	Proteinuria Edema	Hypertension	9.4 g/gCr	2+	1.4	(–)	PSL35 mg/day	HD (3 years after biopsy)
4-2nd [14]	Japanese	M	68	No	Proteinuria Edema	ABO-in-compatible living kidney transplantation 3 month ago	6.8 g/gCr	2+	1.75	(–)	Pulse steroid therapy	Death due to Legionella pneumonia (8 months after transplantation)
Our case – 1st	Japanese	M	77	No	Proteinuria Edema	Atrial fibrillation, prostate cancer	1.2 g/gCr	20–29 (/HPF)	0.8	(–)	Conservative treatment	Cr 1.78 mg/dL, eGFR 29.5 mL/min/1.73 m^2 (2 years after biopsy)
Our case – 2nd	Japanese	M	79	No	Proteinuria Edema	Atrial fibrillation, prostate cancer	11.3 g/gCr	>100 (/HPF)	2.06	(–)	PSL50 mg/day	HD (7 months after second biopsy)

Case	Light microscopy	Electron-dense bands in width/center to center distance	IF on frozen tissue	IF/IHC on FFPE	Electron-dense deposits
(b)					
1 [10]	MPGN pattern	10 nm/32 nm	IgM, C1q, C3 in Mes, CW	Fibrinogen (+)	Subendothelial Mesangium Subepithelial
2 [11]	MPGN pattern	ND	All negative	ND	Subendothelial Mesangium
3 [12]	MPGN pattern	10–12 nm/30–32 nm	C3, C1q in Mes, CW	ND	Subendothelial Mesangium Subepithelial
4-1st [13]	MPGN pattern	10–12 nm/25–30 nm	IgG, IgM, C3, C1q, fibrinogen in Mes, CW	PTAH (+)	Subendothelial

Table 2 (continued)

Case	Light microscopy	Electron-dense bands in width/center to center distance	IF on frozen tissue	IF/IHC on FFPE	Electron-dense deposits
			IgGκ in CW		
4-2nd [14]	MPGN pattern	10–12 nm/25–30 nm	All negative	IgGκ (+)	Subendothelial
Our case – 1st	MPGN pattern	10 nm/20–30 nm	IgM, C3, fibrinogen in CW	Fibrinogen (+), fibrin (+) Fibronectin (+)	Subendothelial
Our case – 2nd	MPGN pattern	10 nm/20–30 nm	IgM, C3, fibrinogen in CW	Fibrinogen (+), fibrin (+) Fibronectin (+)	Subendothelial

ND, no data; HD, hemodialysis. MPGN, membranoproliferative glomerulonephritis; ND, no data; IF, immunofluorescence; Mes, mesangial area; CW, capillary wall; IHC, immunohistochemistry; FFPE, formalin-fixed paraffin-embedded; PTAH, phosphotungstic acid hematoxylin.

consistent with those of collagenofibrotic glomerulopathy and fibronectin nephropathy. With the appearance of microtubular substructures, cryoglobulinemic glomerulonephritis is considered to be one of the most important differential diagnoses. Cryoglobulin tests were negative but not sufficient to exclude cryoglobulinemic glomerulonephritis because they are often false-negative.

The clinical features of cryoglobulinemia, such as joint pain, skin ulcer, purpura, and Raynaud's symptoms, were not observed in the present case. The underlying diseases associated with cryoglobulinemic nephropathy, such as hepatitis C, hepatitis B, autoimmune diseases including SLE and Sjogren's disease, or blood disorders were excluded by serological blood tests and bone marrow biopsy. The pathological findings characteristic of cryoglobulinemic nephropathy, such as intraluminal thrombi, cryoglobulinemic vasculitis, and cryoglobulin plugs, were not present.

Finally, based on pathological and clinical findings, we excluded diseases with organized deposits, such as cryoglobulinemic glomerulonephritis, cryofibrinogen-associated glomerulonephritis, immunotactoid glomerulonephritis, fibrillary glomerulonephritis, lupus nephritis, collagenofibrotic glomerulopathy, fibronectin nephropathy, nail patella syndrome, diabetic fibrillosis [8], and type VI collagen-related nephropathy [9].

We reviewed four previously reported cases with striated ultrastructural deposits [10–14] and examined their clinical and pathological characteristics (Table 2). Cases 4-1st and 4-2nd were from the same patient who underwent two renal biopsies. All cases were reported in Japan and included three men and one woman. None of the patients had a relevant family history and all presented with edema, proteinuria, and hematuria. No hematologic disorders were detected in any of the cases (Table 2a). All patients showed the characteristic MPGN pattern on light microscopy (Table 2b). The striated ultrastructure deposition was detected in the subendothelial space in all cases, in the subepithelial region in two cases, and the mesangial region in three cases. The electron-dense bands were 10–12 nm wide with a distinctive periodicity of approximately 25–30 nm. IF findings varied from negative to positive. Three patients showed immunoglobulins and complement in the capillary wall and mesangial regions.

All patients were resistant to steroid therapy and started hemodialysis within 3 years of renal biopsy (Table 2a). The patient in case 4 had undergone ABO-incompatible living kidney transplantation 2 years after hemodialysis was initiated [14]. Although he was treated with immunosuppressive drugs, including prednisolone, tacrolimus, and mycophenolate mofetil, his serum creatinine level

increased from 1.29 to 2.37 mg/dL 3 weeks after transplantation. The renal biopsy of the allograft kidney showed the striated ultrastructural deposits similar to that observed in the initial biopsy, indicating disease recurrence. This clinical course suggests that some humoral factors contribute to the development of glomerulonephritis, and immunosuppressive therapies are ineffective for glomerulonephritis with striated ultrastructural deposits.

The underlying mechanisms and factors of striated ultrastructure formation remain unknown. To our knowledge, this is the first report of MS analysis used to determine the composition of striated ultrastructural deposits. Fibrinogen and fibronectin were detected at high levels. According to previous reports, fibrinogen levels are not elevated in normal glomeruli or in glomerulonephritis such as amyloidosis, IgA nephropathy, membranous nephropathy, fibrillary glomerulonephritis, immunotactoid glomerulonephritis, and cryoglobulinemic glomerulonephritis, except fibrinogen-α-amyloidosis and cryofibrinogen-associated glomerulonephritis [15–17]. In contrast, fibronectin is detected at low levels in normal glomeruli by MS, and fibronectin levels are elevated in immunotactoid glomerulonephritis and cryoglobulinemic glomerulonephritis, as in our case [15, 17].

In our case, immunostaining for fibrin, fibronectin, and fibrinogen was positive in the subendothelial space, consistent with the location of the deposits. Because MS detects homologous proteins as identical proteins [18], fibrin was detected as fibrinogen, not as a separate protein. We additionally present unpublished data of MS results from a previously reported case (case 1), provided by National Hospital Organization Kyoto Medical Center, which also showed that fibrinogen and fibronectin levels were significantly increased (Fig. 2b). Furthermore, we estimated the absolute protein amount from our case and case 1 by emPAI, which confirmed that fibrinogen and fibronectin were significantly increased (Fig. 2a, b). These results strongly support the possibility that fibrinogen and fibronectin are involved in the structure.

A previous report showed that fibrin has a band pattern with a periodic structure measuring 22.5 ± 1.0 nm [19], similar to the structures in our case. Fibronectin also plays an important role in fibrin formation. Fibronectin strengthens the structure of fibrin and increases its stability by binding to it [20–22]. Therefore, we speculated that the striated ultrastructure is composed of a fibrin-fibronectin complex, and that the accumulation of these complexes induces endothelial injury, leading to MPGN. The causes of fibrinogen/fibrin deposition may involve humoral factors, abnormal coagulation capacity, or intraglomerular environments that are unable to break down the fibrin-fibronectin complex [23, 24]. Further studies are required to elucidate the underlying pathogenesis of this condition.

We report glomerulonephritis with striated ultrastructural deposits, which is inconsistent with any of the known disease deposits. MS analysis and emPAI indicates that the striated ultrastructure deposits could be composed of a fibrin-fibronectin complex, and that the accumulation of fibrin-fibronectin complexes induces endothelial injury, leading to MPGN. Clinicians should be aware of the findings of glomerulonephritis with striated ultrastructural deposits because these patients are nonresponsive to steroids and have a poor prognosis.

Acknowledgments

We thank Shigeo Hara, Tomoko Namba-Hamano, Masaya Saito, Tatsuo Yamamoto, and Hiroyasu Tsukaguchi for providing clinical and pathological information (Table 2).

Statement of Ethics

This study was approved by the Ethics Committees of Kyoto University Hospital, Approved No. 562. This case report was written in compliance with the Declaration of Helsinki. The patient has signed the informed consent for publication.

Conflict of Interest Statement

The authors have no conflicts of interest to declare.

Funding Sources

No funding was received for this study.

Author Contributions

Manna Ishida and Shinya Yamamoto performed primary manuscript preparation; Manna Ishida, Yohei Iwashige, and Shinya Yamamoto wrote the manuscript. Shinya Yamamoto had primary responsibility for the final content; and Manna Ishida, Shinya Yamamoto, Yohei Iwashige, Shuma Miyazawa, Hirosuke Nakata, Seta Koichi, Kensei Yahata, Sachiko Minamiguchi, Yoko Endo, Akiko Mii, Akira Shimizu, and Motoko Yanagita reviewed the manuscript, revised it critically, and approved the final manuscript.

Data Availability Statement

The dataset supporting the conclusions of this article is included within the article.

References

1 Herrera GA, Turbat-Herrera EA. Renal diseases with organized deposits: an algorithmic approach to classification and clinicopathologic diagnosis. Arch Pathol Lab Med. 2010;134(4):512–31. https://doi.org/10.5858/134.4.512

2 Alan SLY, Chertow GM, Luyckx VA, Marsden PA, Skorecki K, Taal MW, et al. Brenner & Rector's THE KIDNEY eleventh edition, [chapter 31]. p. 1069.

3 Sethi S, Palma LMP, Theis JD, Fervenza FC. Proteomic analysis of complement proteins in glomerular diseases. Kidney Int Rep. 2023;8(4):827–36. https://doi.org/10.1016/j.ekir.2023.01.030

4 Vrana JA, Gamez JD, Madden BJ, Theis JD, Bergen HR 3rd, Dogan A. Classification of amyloidosis by laser microdissection and mass spectrometry-based proteomic analysis in clinical biopsy specimens. Blood. 2009;114(24):4957–9. https://doi.org/10.1182/blood-2009-07-230722

5 Gonzalez Suarez ML, Zhang P, Nasr SH, Sathick IJ, Kittanamongkolchai W, Kurtin PJ, et al. The sensitivity and specificity of the routine kidney biopsy immunofluorescence panel are inferior to diagnosing renal immunoglobulin-derived amyloidosis by mass spectrometry. Kidney Int. 2019;96(4):1005–9. https://doi.org/10.1016/j.kint.2019.05.027

6 Ishihama Y, Oda Y, Tabata T, Sato T, Nagasu T, Rappsilber J, et al. Exponentially modified protein abundance index (emPAI) for estimation of absolute protein amount in proteomics by the number of sequenced peptides per protein. Mol Cel Proteomics. 2005;4(9):1265–72. https://doi.org/10.1074/mcp.M500061-MCP200

7 Aoki M, Kang D, Katayama A, Kuwahara N, Nagasaka S, Endo Y, et al. Optimal conditions and the advantages of using laser microdissection and liquid chromatography tandem mass spectrometry for diagnosing renal amyloidosis. Clin Exp Nephrol. 2018;22(4):871–80. https://doi.org/10.1007/s10157-018-1533-y

8 Sohar E, Ravid M, Ben-Shaul Y, Reshef T, Gafni J. Diabetic fibrillosis. A report of three cases. Am J Med. 1970;49(1):64–9. https://doi.org/10.1016/s0002-9343(70)80114-0

9 Mori M, Katayama K, Joh K, Ishikawa E, Dohi K. Type VI collagen-related nephropathy. Clin Kidney J. 2023;16(1):195–6. https://doi.org/10.1093/ckj/sfac126

10 Yahata K, Kikuchi Y, Koizumi M, Seta K, Wakui H, Komatsuda A, et al. Membranoproliferative glomerulonephritis with unusual deposits of parallel arrangement striated structure: a new pathological entity? Clin Nephrol. 2018;89(2):123–9. https://doi.org/10.5414/CN109169

11 Yamamoto T, Togawa A, Eguchi M, Ohashi N, Yasuda H, Harita Y, et al. Glomerulopathy with distinctive fibrillar deposits but lacking glomerular deposition of type III collagen. CEN Case Rep. 2016;5(2):163–7. https://doi.org/10.1007/s13730-016-0217-2

12 Ohtani H, Wakui H, Komatsuda A, Goto H, Tada M, Ozawa M, et al. Progressive glomerulopathy with unusual deposits of striated structures: a new disease entity? Nephrol Dial Transpl. 2010;25(6):2016–9. https://doi.org/10.1093/ndt/gfq037

13 Hara S, Tsukaguchi H, Oka T, Kusabe M, Mizui M, Joh K. Monoclonal immunoglobulin-associated proliferative glomerulonephritis characterized by organized deposits of striated ultra-substructures: a case report. Ultrastruct Pathol. 2017;41(4):301–7. https://doi.org/10.1080/01913123.2017.1336189

14 Namba-Hamano T, Hamano T, Imamura R, Yamaguchi Y, Kyo M, Yonishi H, et al. Recurrence of proliferative glomerulonephritis with monoclonal immunoglobulin G deposits with a striated ultrastructure. Nephron. 2020;144(Suppl 1):43–8. https://doi.org/10.1159/000512330

15 Sethi S, Theis JD, Vrana JA, Fervenza FC, Sethi A, Qian Q, et al. Laser microdissection and proteomic analysis of amyloidosis, cryoglobulinemic GN, fibrillary GN, and immunotactoid glomerulopathy. Clin J Am Soc Nephrol. 2013;8(6):915–21. https://doi.org/10.2215/CJN.07030712

16 Ibuki E, Shiraishi A, Sofue T, Kushida Y, Kadota K, Honda K, et al. Characteristic electron-microscopic features of cryofibrinogen-associated glomerulonephritis: a case report. BMC Nephrol. 2020;21(1):27. https://doi.org/10.1186/s12882-020-1696-0

17 Kawata N, Kang D, Aiuchi T, Obama T, Yoshitake O, Shibata T, et al. Proteomics of human glomerulonephritis by laser microdissection and liquid chromatography-tandem mass spectrometry. Nephrology. 2020;25(4):351–9. https://doi.org/10.1111/nep.13676

18 Shuken SR. An introduction to mass spectrometry-based proteomics. J Proteome Res. 2023;22(7):2151–71. https://doi.org/10.1021/acs.jproteome.2c00838

19 Weisel JW. The electron microscope band pattern of human fibrin: various stains, lateral order, and carbohydrate localization. J Ultrastruct Mol Struct Res. 1986;96(1–3):176–88. https://doi.org/10.1016/0889-1605(86)90019-4

20 Okada M, Blombäck B, Chang MD, Horowitz B. Fibronectin and fibrin gel structure. J Biol Chem. 1985;260(3):1811–20. https://doi.org/10.1016/s0021-9258(18)89665-x

21 Wang Y, Reheman A, Spring CM, Kalantari J, Marshall AH, Wolberg AS, et al. Plasma fibronectin supports hemostasis and regulates thrombosis. J Clin Investig. 2014;124(10):4281–93. https://doi.org/10.1172/JCI74630

22 Lemańska-Perek A, Krzyżanowska-Gołąb D, Pupek M, Klimeczek P, Witkiewicz W, Kątnik-Prastowska I. Analysis of soluble molecular fibronectin-fibrin complexes and EDA-fibronectin concentration in plasma of patients with atherosclerosis. Inflammation. 2016;39(3):1059–68. https://doi.org/10.1007/s10753-016-0336-0

23 Kattula S, Byrnes JR, Wolberg AS. Fibrinogen and fibrin in hemostasis and thrombosis. Arterioscler Thromb Vasc Biol. 2017;37(3):e13–21. https://doi.org/10.1161/ATVBAHA.117.308564

24 Weisel JW, Litvinov RI. Fibrin Formation, structure and properties. Subcell Biochem. 2017;82:405–56. https://doi.org/10.1007/978-3-319-49674-0_13